Supplement of Atmos. Chem. Phys., 26, 1483–1496, 2026
https://doi.org/10.5194/acp-26-1483-2026-supplement

Atmospheric Chemistry and Physics
Open Access
EGU

Supplement of

Divergent iron dissolution pathways controlled by sulfuric and nitric acids from the ground-level to the upper mixing layer

Guochen Wang et al.

Correspondence to: Weijun Li (liweijun@zju.edu.cn)

S1. Sensitivity analysis of size-resolved aerosol pH to ammonia

Previous studies have revealed that ammonia (NH_3) is a key alkaline gas influencing aerosol pH and that its absence in field measurements can introduce uncertainty (Hennigan et al., 2015; Song et al., 2018). Since ambient 2021 NH_3 at the upper mixing layer (Mt. Daming) was not measured during the field campaign, we adopted ambient NH_3 in 2025 to present its concentration. To evaluate the sensitivity of pH to the assumed NH_3 level in size-resolved aerosols, we conducted a sensitivity analysis by varying NH_3 concentrations over an order of magnitude while holding all other parameters constant (Fig. S3). The results showed that two times (4 ppb) change in NH_3 can increase pH with 0.2 unit and a ten-fold (20 ppb) change in NH_3 induces approximately a 1-unit change in aerosol pH—consistent with previous modeling studies (Guo et al., 2015; Guo et al., 2017; Weber et al., 2016). Given the relatively clean background environment at our mountain sampling site, the NH_3 emissions is expected to exhibit minimal variation over the short sampling period, thus, the assumed NH_3 concentration is likely conservative and within reasonable bounds. Therefore, while we acknowledge the potential uncertainty due to the 2025 NH_3 measurements, we believe the simulated aerosol pH values are sufficiently representative for investigating proton-promoted processes such as Fe dissolution.

S2. Atmospheric chemical transport model

Since size-resolved aerosol data were unavailable for Hangzhou, we simulated size-fractionated iron solubility using the Integrated Massively Parallel Atmospheric Chemical Transport (IMPACT) model (Ito and Miyakawa, 2023; Ito et al., 2019; Ito and Xu, 2014). The simulations were conducted at a horizontal resolution of 2.0° × 2.5° with 47 vertical layers, covering the observation period from September 11 to 21, 2021 (Hangzhou). The model was driven by MERRA-2 reanalysis meteorological data provided by NASA's Global Modeling and Assimilation Office (GMAO). IMPACT model simulates the emission, chemistry, transport, and deposition of aerosols and their precursors from anthropogenic, pyrogenic, lithogenic, oceanic, and biogenic sources. Iron solubility over Hangzhou was estimated for two aerosol size bins (D_p <1 μm and D_p >1 μm).

As shown in Fig. S6a−b, the model reproduces both the magnitude and relative contributions of sulfate and nitrate reasonably well, indicating that it captures the dominant acidifying components controlling aerosol acidity at this site. While the model slightly overestimates Fe solubility (%Fe_S) compared to observations (Fig. S6c), the discrepancy remains within one order of magnitude (± 10). The model also captures the elevated %Fe_S. The overestimation is likely due to a size mismatch: the model simulates %Fe_S for the D_p >1 μm fraction, whereas the observations are based on total suspended particles (TSP), which include a broader particle size range.

S3. Limited role of ligand-promoted pathway in Fe dissolution

While organic acids can contribute to iron solubilization, their concentrations are generally much lower than those of strong inorganic acids such as sulfuric and nitric acids. For example, Deshmukh et al. (2023) reported that oxalate-to-sulfate and oxalate-to-nitrate mass ratios of approximately 1:25 and 1:4, respectively, in fine particles (D_p <1 μm), and ~1:16 and ~1:18 in coarse particles (D_p >1 μm). In this study, oxalate concentrations in TSP were estimated following an empirical relationship $\left(\left[C_2O_4^{2-}\right] = 0.05 \times \left[SO_4^{2-}\right] - 0.273\right)$ proposed by Yu et al. (2005), yielding oxalate-to-(sulfate + nitrate) ratios of ~6% at the mountain site and ~5% at Hangzhou, respectively. At such low concentrations, we believe that the contribution of organic acids to iron dissolution is limited. What's more, our recent research (Li et al., 2025) also revealed that oxalate, like Ca^{2+}, was predominantly present in coarse-mode particles, peaking in the 3.2–5.6 μm size bin—consistent with previous findings from Deshmukh et al. (2023). Since our study focused on TSP samples with larger particle size, the relative contribution of organic acids to Fe dissolution is expected to be low due to their relatively low loadings in the coarse fraction.

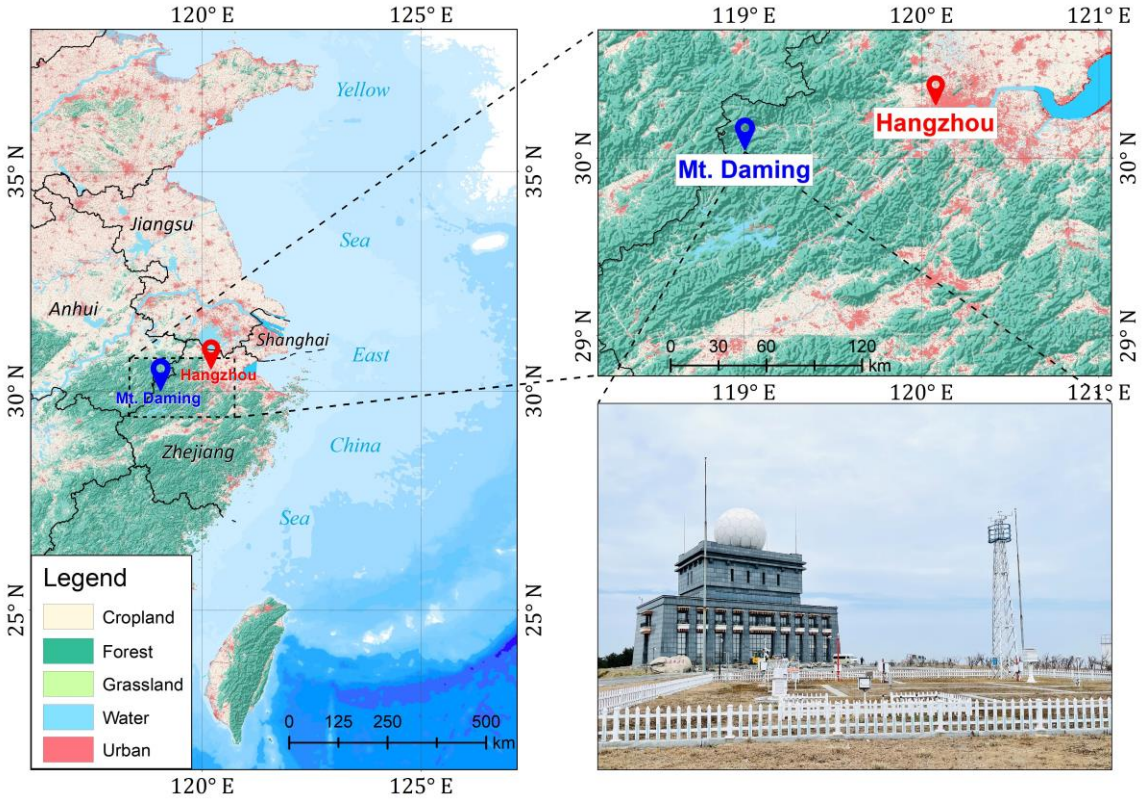

Figure S1. Map of the sampling sites. The symbols in the upper-right panel indicate the locations of the upper mixing layer (Mt. Daming; 30.03° N, 119.00° E; 1483 m) and the ground-level of Hangzhou (30.30° N, 120.09° E; 6 m), respectively. The photograph in the lower-right panel was taken at the entrance of the Mt. Daming station. The background map shows land-use types of China in 2022 at a spatial resolution of 30 m (Yang and Huang, 2021). Map: Esri | Powered by Esri.

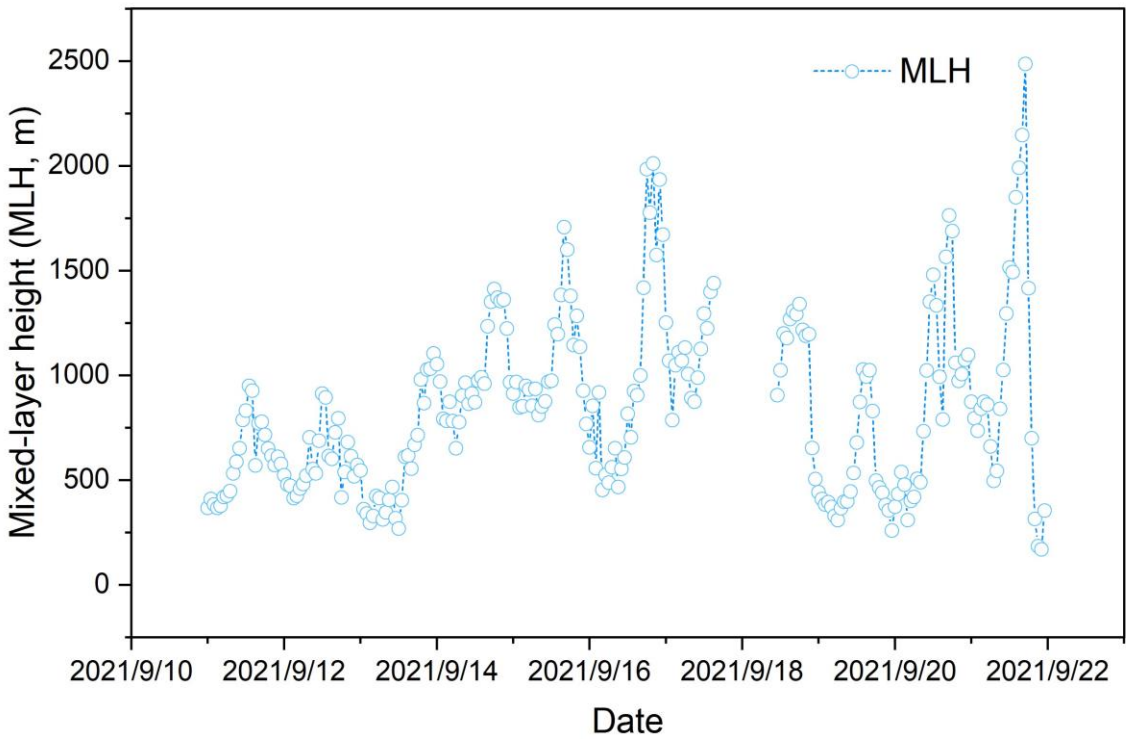

Figure S2. Time series of mixed-layer height (MLH) in Hangzhou during the sampling period (September 11 to 21, 2021).

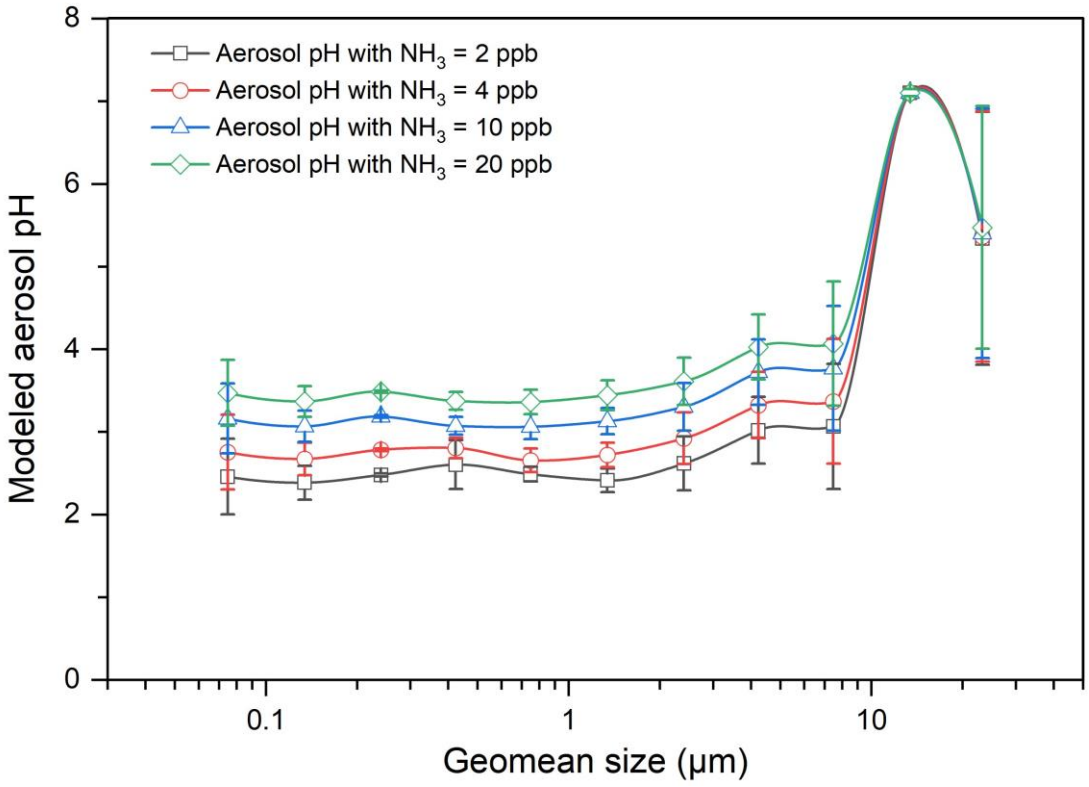

Figure S3. Modeled aerosol pH for the Mt. Daming across different particle size bins under varying NH_3 concentrations (2, 4, 10, and 20 ppb), simulated using the ISORROPIA II model. The lowest NH_3 concentration (~2 ppb) represents the average level observed during the 2025 field campaign. The pH was calculated based on measured inorganic composition and assumed thermodynamic equilibrium under metastable conditions. Error bars represent the standard deviation of pH values within each size bin (n = 3).

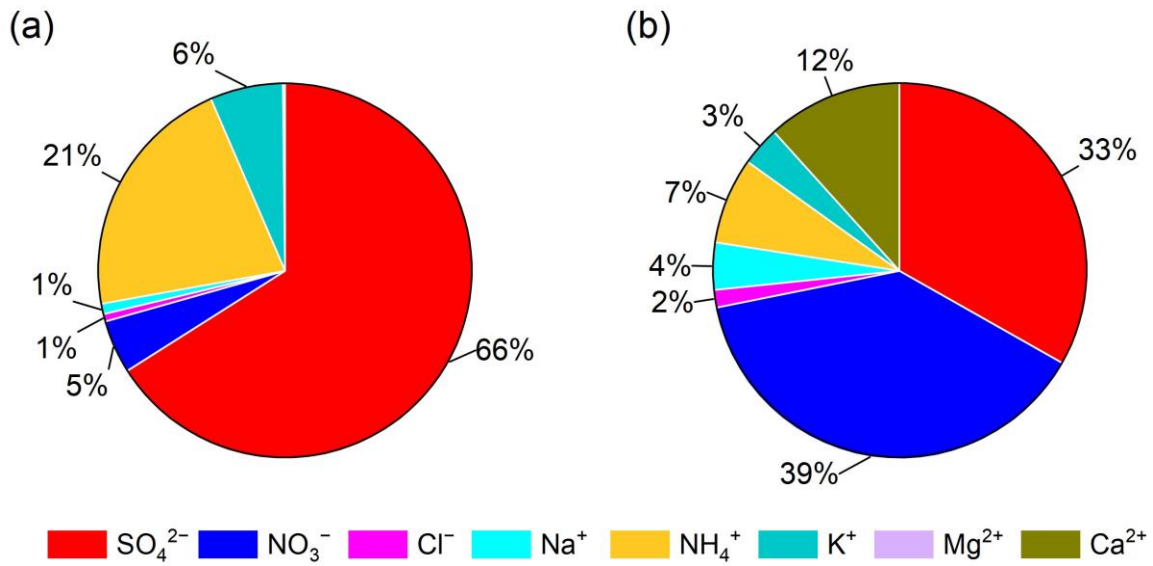

Figure S4. Percentage of the measured water-soluble inorganic ions in the sized-resolved aerosols collected in the upper mixing layer of Mt. Daming. Panels show (**a**) the submicron particles (D_p <1 μm) and (**b**) the supermicron particles (D_p >1 μm), respectively.

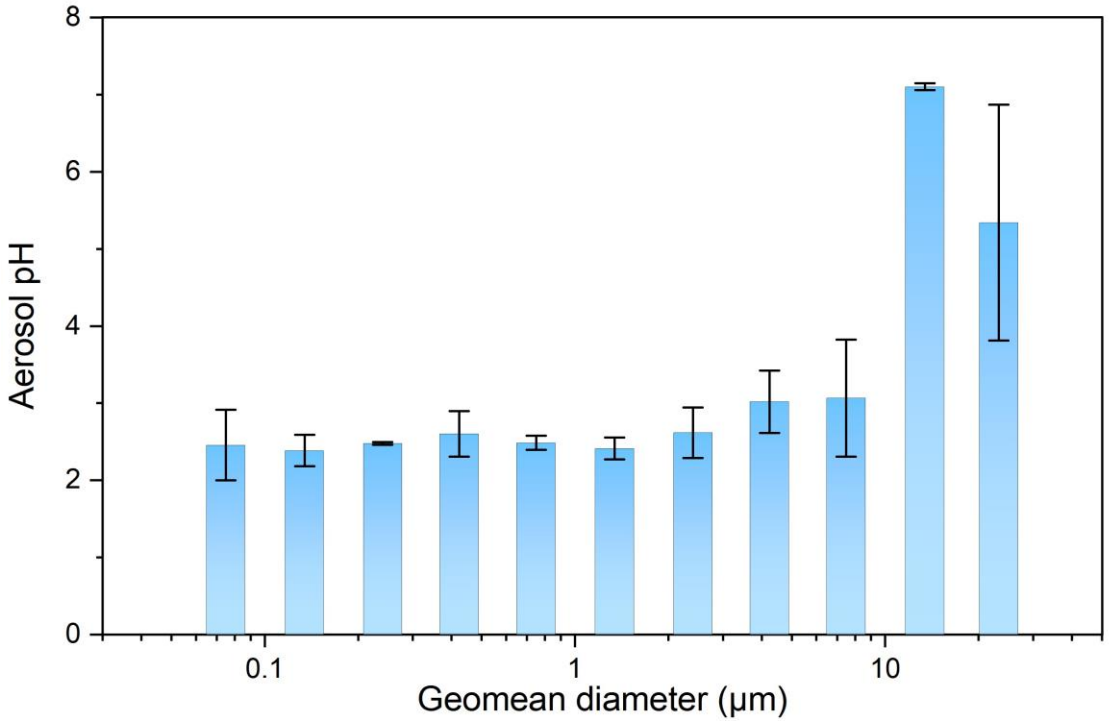

Figure S5. Aerosol pH simulated using ISORROPIA II model for size-resolved aerosols in the upper mixing layer (Mt. Daming). Vertical bars represent one standard deviation (*n* = 3).

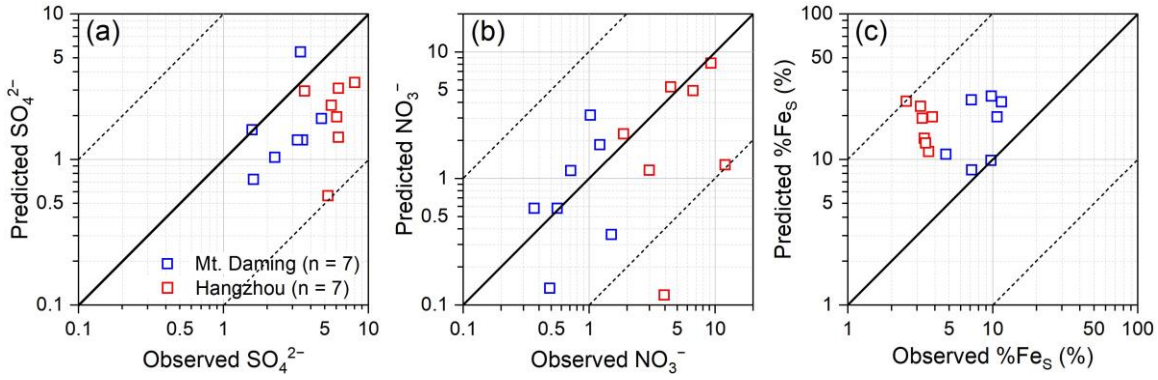

Figure S6. Comparison of observed SO_4^{2-}, NO_3^-, and Fe solubility ($\%Fe_S$) in TSP with those predicted by the Integrated Massively Parallel Atmospheric Chemical Transport (IMPACT) model over Hangzhou city. Panels show (**a**) SO_4^{2-}, (**b**) NO_3^-, and (**c**) $\%Fe_S$. The solid line represents the 1:1 reference line. The dashed lines denote deviations from the solid line by a factor of ± 10.

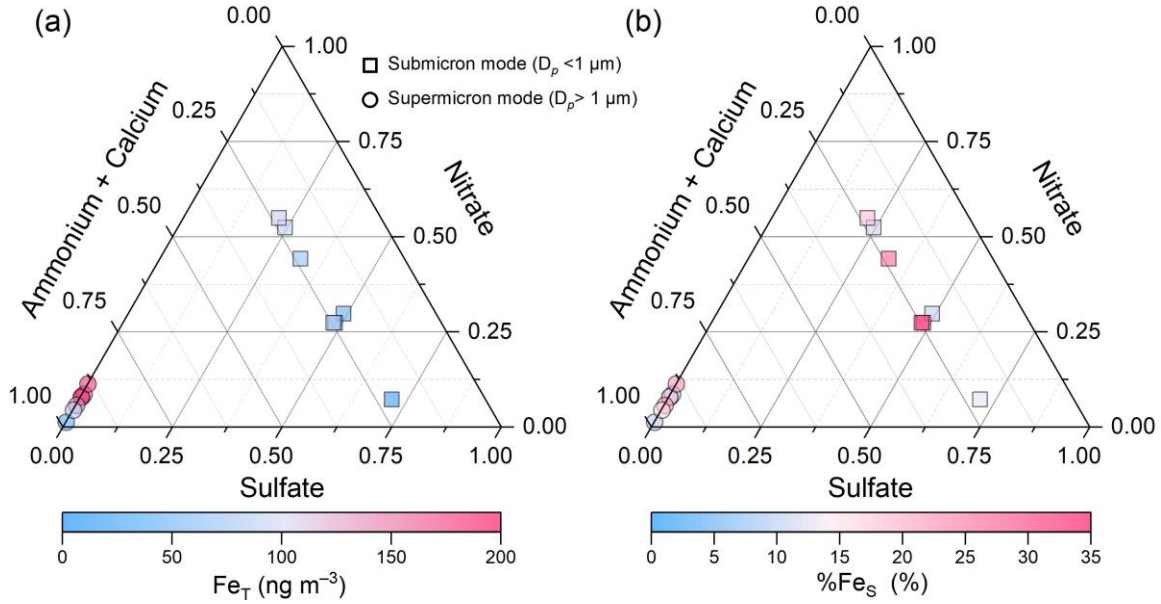

Figure S7. Ternary diagram showing the relative abundances of sulfate, nitrate, and alkaline species (ammonium + calcium) in size-resolved aerosols simulated for Hangzhou using the IMPACT model. The symbols (circles and squares) are colored by total Fe (Fe_T) in panel (**a**) and by $\%Fe_S$ in panel (**b**).

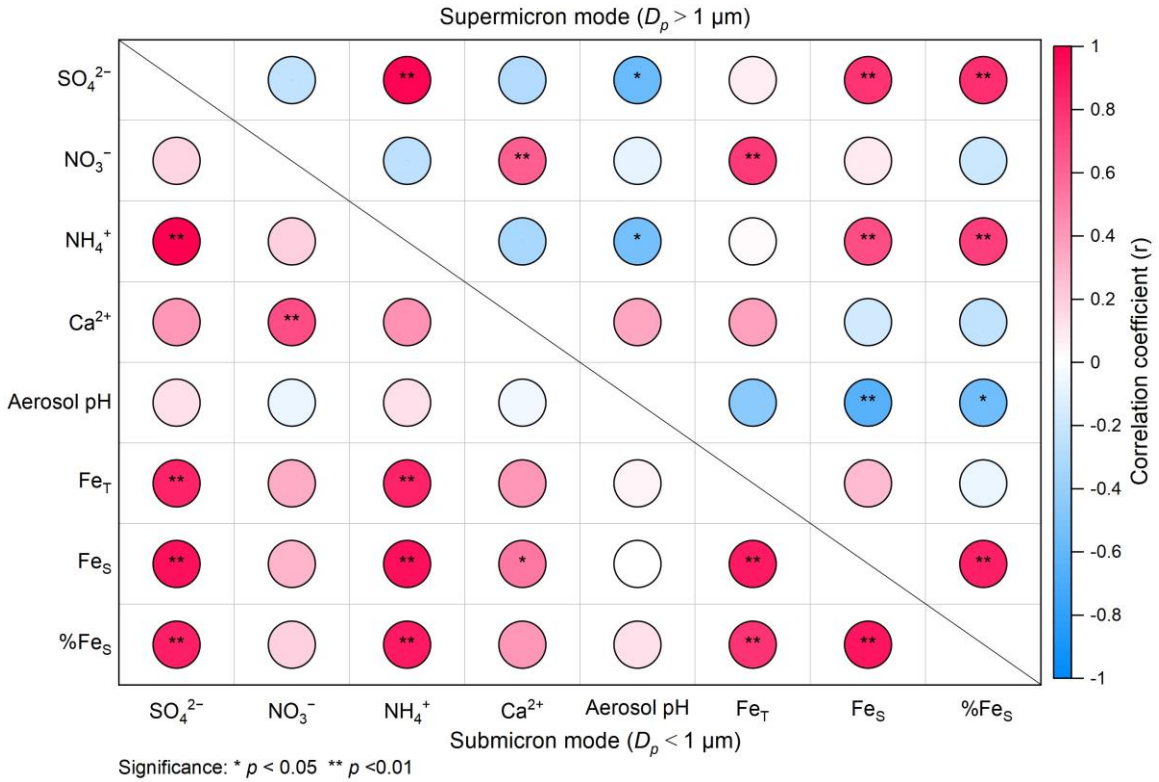

Figure S8. Pearson correlation matrix of aerosol chemical components (SO_4^{2-}, NO_3^-, NH_4^+, and Ca^{2+}), Fe_T, Fe_S, %Fe_S, and aerosol pH in size-resolved aerosols at Mt. Daming. Filled circles are colored according to the correlation coefficients. "*" indicates *p*-values less than 0.05 ($p < 0.05$) and "**" means *p*-values less than 0.01 ($p < 0.01$).

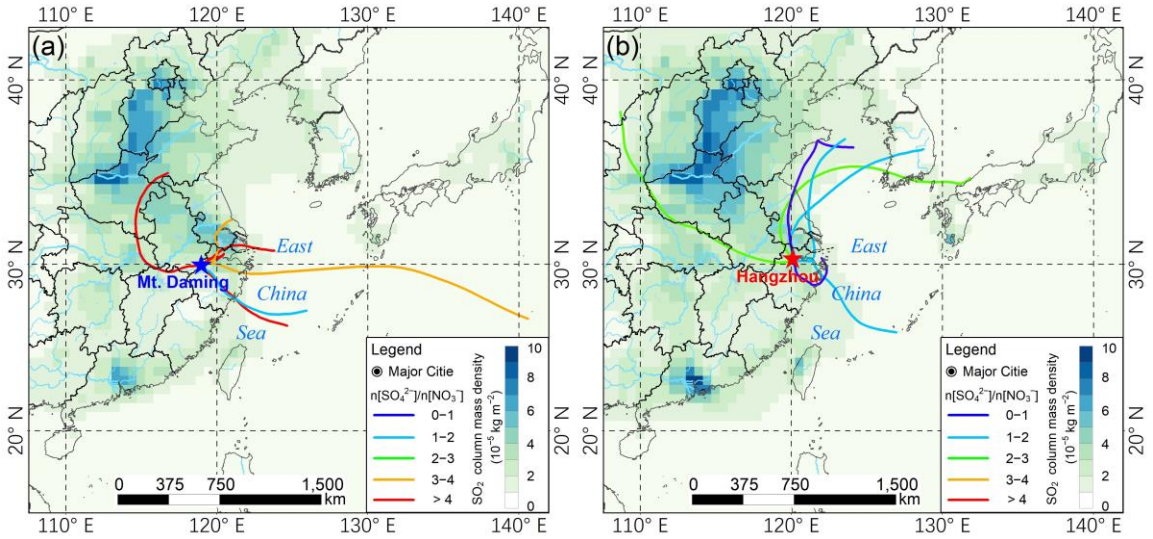

Figure S9. Backward trajectories overlaid on SO_2 column mass density maps during the sampling period. (**a**) the upper mixing layer (Mt. Daming), and (**b**) Hangzhou. The color shading indicates the hourly averaged SO_2 column mass density (in 10^{-5} kg m^{-2}) with a spatial resolution of 0.5° × 0.625°, retrieved from Goddard Earth Sciences Data and Information Services Center (GES DISC) (available at https://giovanni.gsfc.nasa.gov/giovanni/, accessed on June 3, 2025). Lines show 48-hour backward trajectories at 500 m altitude calculated using the HYSPLIT model. Line colors represent the molar ratios of sulfate to nitrate ($n[SO_4^{2-}]/n[NO_3^-]$) along the corresponding air mass transport pathway.

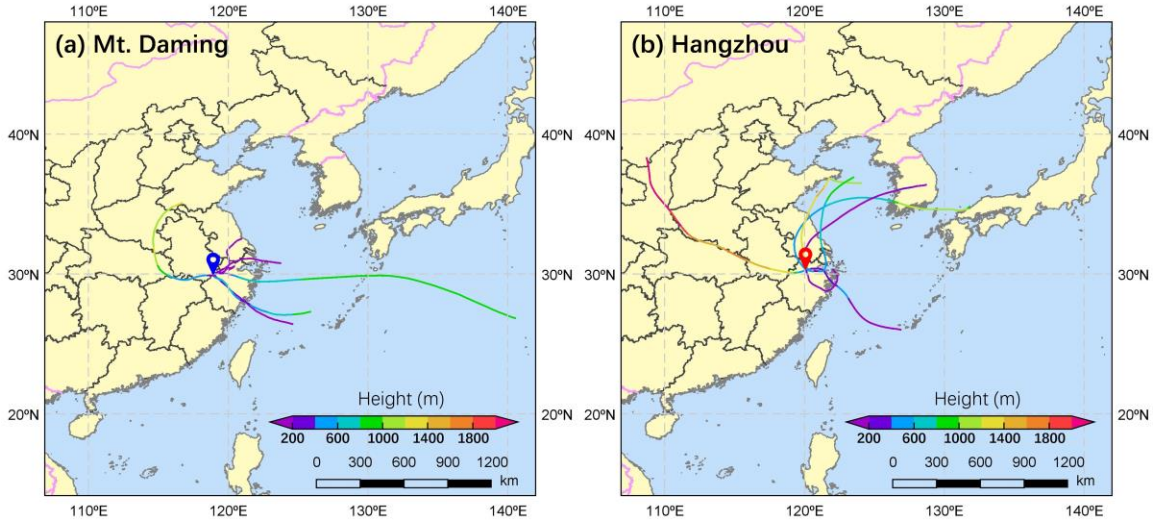

Figure S10. The heights of 48-hour backward trajectories arriving at (**a**) the upper mixing layer (Mt. Daming) and (**b**) Hangzhou. Heights are given in meters (m).

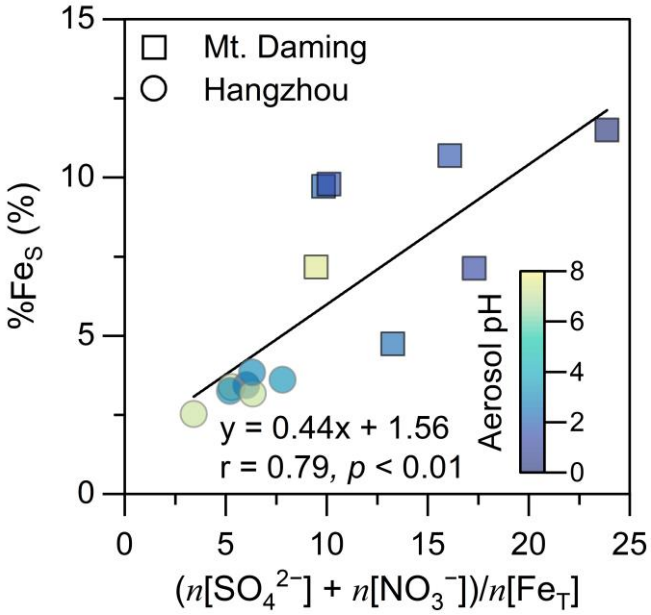

Figure S11. Correlations between $\%Fe_S$ and the corresponding molar ratio of ($n[SO_4^{2-}]$ + $n[NO_3^-]$)/$n[Fe_T]$ at Mt. Daming and Hangzhou. Data points (solid circles and squares) are colored according to aerosol pH.

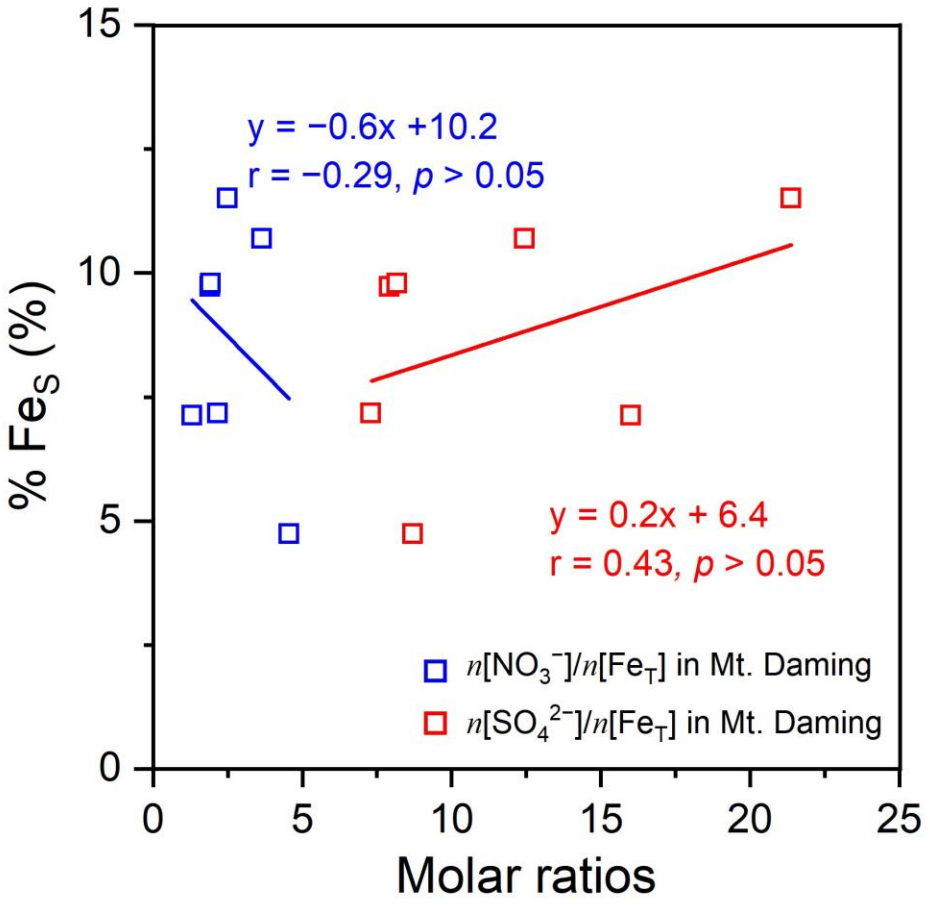

Figure S12. Correlations between $\%Fe_S$ and $n[SO_4^{2-}]/n[Fe_T]$ or $n[NO_3^-]/n[Fe_T]$ molar ratios at Mt. Daming. Linear regression lines are shown for each relationship.

Table S1. Sampling information (sampling site, number, sample time, mean temperature and relative humidity) during the field campaign.

Sampling site	NO.	Sampling time	Mean temperature (℃)	Mean relative humidity (%)
Mt. Daming	M1	2021/7/17	20.88	95.63
	M2	2021/7/18-7/19*	19.40	94.68
	M3	2021/7/20-7/21*	20.49	91.47
	M4	2021/7/29-8/1*	26.90	82.97
	M5	2021/8/2	22.19	83.00
	M6	2021/8/8-8/9*	21.46	81.96
	M7	2021/8/12-8/19*	19.58	87.28
Hangzhou	H1	2021/9/11	27.08	82.18
	H2	2021/9/14	25.44	78.16
	H3	2021/9/16	24.76	79.48
	H4	2021/9/17	25.50	66.00
	H5	2021/9/18	25.87	61.80
	H6	2021/9/19	27.77	67.22
	H7	2021/9/21	27.60	58.68

Note: "*" indicates that the sampling was temporarily stopped due to rain events during the sampling period.

References

Deshmukh, D. K., Kawamura, K., Kobayashi, M., and Gowda, D.: Changes in the Size Distributions of Oxalic Acid and Related Polar Compounds Over Northern Japan During Spring, J. Geophys. Res.: Atmos., 128, e2022JD038461, https://doi.org10.1029/2022jd038461, 2023.

Guo, H., Weber, R. J., and Nenes, A.: High levels of ammonia do not raise fine particle pH sufficiently to yield nitrogen oxide-dominated sulfate production, Sci. Rep., 7, 12109, https://doi.org10.1038/s41598-017-11704-0, 2017.

Guo, H., Xu, L., Bougiatioti, A., Cerully, K. M., Capps, S. L., Hite, J. R., Carlton, A. G., Lee, S. H., Bergin, M. H., Ng, N. L., Nenes, A., and Weber, R. J.: Fine-particle water and pH in the southeastern United States, Atmos. Chem. Phys., 15, 5211–5228, https://doi.org10.5194/acp-15-5211-2015, 2015.

Hennigan, C. J., Izumi, J., Sullivan, A. P., Weber, R. J., and Nenes, A.: A critical evaluation of proxy methods used to estimate the acidity of atmospheric particles, Atmos. Chem. Phys., 15, 2775–2790, https://doi.org10.5194/acp-15-2775-2015, 2015.

Ito, A. and Miyakawa, T.: Aerosol Iron from Metal Production as a Secondary Source of Bioaccessible Iron, Environ. Sci. Technol., 57, 4091−4100, https://doi.org10.1021/acs.est.2c06472, 2023.

Ito, A. and Xu, L.: Response of acid mobilization of iron-containing mineral dust to improvement of air quality projected in the future, Atmos. Chem. Phys., 14, 3441−3459, https://doi.org10.5194/acp-14-3441-2014, 2014.

Ito, A., Myriokefalitakis, S., Kanakidou, M., Mahowald, N. M., Scanza, R. A., Hamilton, D. S., Baker, A. R., Jickells, T., Sarin, M., Bikkina, S., Gao, Y., Shelley, R. U., Buck, C. S., Landing, W. M., Bowie, A. R., Perron, M. M. G., Guieu, C., Meskhidze, N., Johnson, M. S., Feng, Y., Kok, J. F., Nenes, A., and Duce, R. A.: Pyrogenic iron: The missing link to high iron solubility in aerosols, Sci. Adv., 5, eaau7671, https://doi.org10.1126/sciadv.aau7671, 2019.

Li, W. J., Ito, A., Wang, G. C., Zhi, M. K., Xu, L., Yuan, Q., Zhang, J., Liu, L., Wu, F., Laskin, A., Zhang, D. Z., Zhang, X. Y., Zhu, T., Chen, J. M., Mihalopoulos, N., Bougiatioti, A., Kanakidou, M., Wang, G. H., Hu, H. L., Zhao, Y., and Shi, Z. B.:

Aqueous-phase secondary organic aerosol formation on mineral dust, Natl. Sci. Rev., nwaf221, https://doi.org10.1093/nsr/nwaf221/8154540, 2025.

Song, S., Gao, M., Xu, W., Shao, J., Shi, G., Wang, S., Wang, Y., Sun, Y., and McElroy, M. B.: Fine-particle pH for Beijing winter haze as inferred from different thermodynamic equilibrium models, Atmos. Chem. Phys., 18, 7423–7438, https://doi.org10.5194/acp-18-7423-2018, 2018.

Weber, R. J., Guo, H., Russell, A. G., and Nenes, A.: High aerosol acidity despite declining atmospheric sulfate concentrations over the past 15 years, Nat. Geosci., 9, 282–285, https://doi.org10.1038/ngeo2665, 2016.

Yang, J. and Huang, X.: The 30 m annual land cover dataset and its dynamics in China from 1990 to 2019, Earth Syst. Sci. Data, 13, 3907−3925, https://doi.org10.5194/essd-13-3907-2021, 2021.

Yu, J. Z., Huang, X. F., Xu, J., and Hu, M.: When Aerosol Sulfate Goes Up, So Does Oxalate-Implication for the Formation Mechanisms of Oxalate, Environ. Sci. Technol., 39, 128–133, https://doi.org10.1021/es049559f, 2005.